

# Effect of changing the electrode gap on the spatial and electrical properties of O<sub>2</sub>/CF<sub>4</sub> plasmas

Kristen L. Steffens<sup>a)</sup> and Mark A. Sobolewski

Process Measurements Division, National Institute of Standards and Technology, Gaithersburg, Maryland 20899

(Received 10 April 2002; accepted 28 October 2002; published 19 December 2002)

Planar laser-induced fluorescence (PLIF) measurements were made to determine two-dimensional spatial maps of CF<sub>2</sub> density as a chemical marker of plasma uniformity in 9% O<sub>2</sub>/91% CF<sub>4</sub> chamber-cleaning plasmas. Broadband optical emission and discharge current and voltage measurements were also made and compared to the PLIF results. Measurements were made in a capacitively coupled Gaseous Electronics Conference Reference Cell as pressure was varied from 13 (100 mTorr) to 133 Pa (1000 mTorr) and electrode gap was varied from 2.25 to 0.5 cm. Smaller gaps resulted in increased radial uniformity and extended the pressure range over which CF<sub>2</sub> density and electrical properties remain insensitive to pressure. These effects are explained by a decrease in the bulk plasma resistance at narrower electrode gaps, which changes the path that rf current takes through the discharge, thus affecting where electron heating and CF<sub>2</sub> production occur. These results provide insight into the optimization of chamber-cleaning processes and reactors as well as provide necessary data for validation of plasma simulations.

[DOI: 10.1116/1.1531142]

## I. INTRODUCTION

Fluorocarbon plasmas are widely used by the semiconductor industry for *in situ* cleaning of deposition chambers and for plasma etching of dielectrics. To reduce operating costs and environmentally harmful emissions, these plasmas must be optimized for efficient gas utilization, fast cleaning or etch rates, and desired spatial characteristics. Since spatial variations in cleaning rates on different reactor surfaces are likely related to spatial variations in reactive gas phase species in the plasma, understanding the effect of factors such as pressure, plasma electrical characteristics, and electrode gap size on the reactive species spatial characteristics would aid in the optimization of these plasmas.

To investigate the behavior of the spatial distribution of reactive species in the plasma, a series of experiments<sup>1,2</sup> was initiated in which O<sub>2</sub>/CF<sub>4</sub> and O<sub>2</sub>/C<sub>2</sub>F<sub>6</sub> chamber-cleaning plasmas were studied in the capacitively coupled Gaseous Electronics Conference (GEC) Reference Cell. In each of the studies, planar laser-induced fluorescence (PLIF) was used to measure the two-dimensional (2D) density distribution of the CF<sub>2</sub> radical as a chemical marker of plasma uniformity. CF<sub>2</sub> is an important reactive species in fluorocarbon etching plasmas and has been the focus of many recent experimental studies.<sup>1-10</sup> As discussed in detail in Ref. 4 and references therein, CF<sub>2</sub> has long been known to be correlated with the formation of the fluorocarbon polymer layer which enables selective etching of oxide layers over silicon. Recent experimental work<sup>4</sup> suggests that this occurs by gas-phase concatenation of CF<sub>2</sub> to form higher molecular weight molecules which subsequently deposit. The PLIF technique allows the entire 2D map of the CF<sub>2</sub> density to be collected simultaneously, eliminating the need for multiple point measure-

ments. In addition to the PLIF measurements, broadband plasma emission images were collected. Plasma emission occurs when electron impact dissociation and electronic excitation of species in the plasma results in electronically excited molecular fragments and atoms which subsequently emit. The lifetimes of many of the created excited state fragments are very short ( $61 \pm 3$  ns (Ref. 11) for CF<sub>2</sub>  $A^1B_1(0, 0, 0)$  and  $26.7 \pm 1.8$  ns (Ref. 12) for CF  $A^2\Sigma^+, v'=0$ ) such that the fragments emit before they have a chance to travel away from the region in which they were created. Thus, the spatial distribution of the emission intensity indicates where reactive species, including CF<sub>2</sub>, are created in the plasma. Discharge current and voltage measurements were also made to determine plasma electrical characteristics, including plasma impedances and the magnitude and paths of rf current flow through the plasma. These measurements are necessary both to characterize the state of the plasma as well as to provide an understanding of the optical results. Measurements of rf current flow and optical emission intensity were particularly closely related, because the mechanisms<sup>13</sup> that heat electrons, making emission possible, depend on the current density.

In the initial set of experiments,<sup>1</sup> the pressure dependence of PLIF data was studied and found to be correlated to optical emission and electrical measurements. These results led to an investigation<sup>2</sup> of whether the spatial distribution of CF<sub>2</sub> could be changed by controlling the flow of current through the plasma by means of a variable impedance load connected between the nonpowered electrode and ground. In some commercial reactors, however, the electrode gap is significantly smaller than the gap in the GEC cell used in previous work. To study how a reduction of the electrode gap affects plasma spatial and electrical properties, we performed the experiments presented here, in which we measured PLIF of

<sup>a)</sup>Electronic mail: kristen.steffens@nist.gov

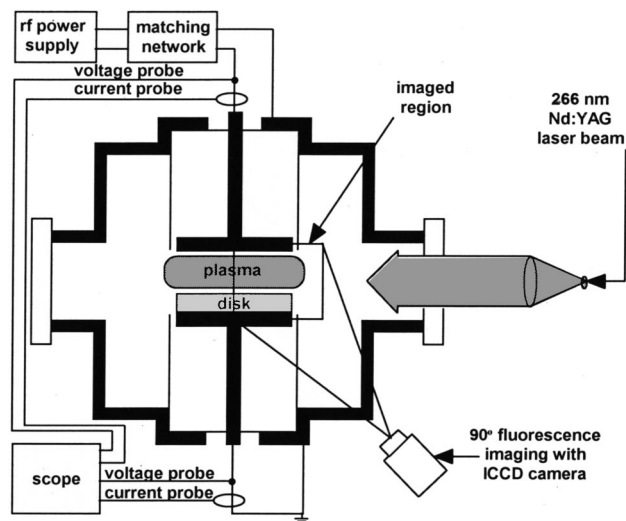


FIG. 1. Experimental schematic of GEC reactor, including spacer disk, electrical probes, and PLIF apparatus.

$\text{CF}_2$ , broadband optical emission, and electrical properties in  $\text{O}_2/\text{CF}_4$  discharges with varying electrode gaps and varying pressures. Correlations between the PLIF, optical emission, and electrical data are noted and discussed. We also present simple analytic models for the electrical impedance of the plasma and its sheaths which provide qualitative explanations of and predictions for the gap dependence and pressure dependence of plasma spatial and electrical properties.

## II. EXPERIMENT

Experiments were conducted in 9%  $\text{O}_2/91\%$   $\text{CF}_4$  chamber-cleaning plasmas at pressures varying from 13 to 133 Pa (100 to 1000 mTorr) and a total gas flow rate of 8.8 standard cubic centimeters per minute in a GEC reference cell.<sup>14</sup> This stainless-steel, parallel-plate, capacitively coupled, rf discharge reactor is equipped with quartz windows and 10.2 cm diameter, water-cooled, aluminum electrodes separated by a gap of 2.25 cm. Each electrode is surrounded by an aluminum oxide insulator and a stainless-steel ground shield. The electrodes are not movable, so the electrode gap was varied by placing anodized aluminum disks of various heights on the lower electrode, as shown in Fig. 1. Because the anodized disks lack a ground shield, we grounded the lower electrode and powered the upper electrode, unlike in previous studies where the lower electrode was powered.<sup>1,2</sup> The upper electrode was powered by a 13.56 MHz power supply, coupled through a matching network. A current probe and a voltage probe were attached to the input power lead. Probes were also mounted on the copper wire that grounded the lower electrode to the exterior of the cell. Using procedures described previously,<sup>15</sup> the stray impedance of the cell was characterized. This characterization allows us to determine the current and voltage at the electrodes, the plasma impedance, and the plasma power, i.e., the power delivered to the discharge itself, excluding all external power losses. Measurements were made at 30 W of plasma

power, which corresponds to a power density which is comparable to industrial reactors operated at hundreds of watts, because of the larger size of industrial reactors and the fact that external losses are usually not taken into account.

The PLIF technique has been discussed in detail previously.<sup>1,16</sup> The 266 nm laser beam from a quadrupled Nd:YAG laser was expanded using cylindrical optics into a vertical laser sheet approximately 2.5 cm tall and 0.5 cm thick. The laser sheet passes through the plasma, exciting the  $\text{CF}_2$  radicals from the X (0, 1, 0) ground electronic state to the A (0, 2, 0) excited electronic state. The laser-excited  $\text{CF}_2$  fluoresces primarily to the X (0, 0-20, 0) states,<sup>11</sup> emitting light between 250 nm and 400 nm. The fluorescence between 300 and 400 nm was imaged normal to the laser sheet, using an intensified charge-coupled device (ICCD) camera with a 105 mm,  $f/4.5$  ultraviolet lens. Colored glass filters reduced broadband plasma emission and blocked the scattered laser light. For each image, up to 1050 laser shots were averaged. In PLIF, the image is not line-of-sight integrated, because only the  $\text{CF}_2$  in the plane of the laser sheet is excited and detected. The spatial resolution was determined by the 5.0 mm laser sheet thickness and the  $0.2\text{ mm} \times 0.2\text{ mm}$  imaged dimensions of the camera pixels.

Broadband, spontaneous plasma emission from multiple species between 300 and 400 nm was measured under the same conditions as for PLIF but with the laser blocked. The emission images were subtracted from each PLIF image before the PLIF images were normalized for spatial variations and drift in the laser intensity, as described previously.<sup>1</sup> In addition, a uniform field correction<sup>16</sup> was applied to the images to normalize for any slight variations in collection efficiency across the ICCD. Care was taken to operate under conditions where the  $\text{CF}_2$  PLIF intensity is proportional to the ground electronic state  $\text{CF}_2$  density, as discussed previously.<sup>1</sup> We verified that collisional quenching does not affect the fluorescence intensity yield, and we used low laser intensities to keep the  $\text{CF}_2$  PLIF signal in the linear regime. Uncertainty in the image-integrated PLIF due to random error is estimated to be  $\pm 6\%$ . Systematic errors could arise due to temperature variations which would cause changes in PLIF intensity due to changes in ground-state rotational and vibrational population distributions, as discussed in detail previously.<sup>1</sup> A weak increase in gas temperature with increasing pressure has been observed in similar plasmas,<sup>17</sup> which would result in a small apparent increase in  $\text{CF}_2$  density. However, under the constant power conditions in this study, effects on these PLIF measurements due to temperature variations are believed to be minor and should be similar for all gaps.

The optical detection for the PLIF is arranged so that, with the full electrode gap of 2.25 cm, there is no vignetting of the fluorescence optical collection volume. However, when the aluminum disks are used to reduce the gap, some optical paths between the plane of the laser sheet and the ICCD lens are obscured. To determine how this affects the  $\text{CF}_2$  PLIF images, PLIF was performed on acetone gas, a technique which has been utilized for flow visualization.<sup>18,19</sup>

The acetone was seeded at 1.7% by volume in air and flowed through the cell at 46.7 kPa (350 Torr) total cell pressure, with no plasma ignited. The acetone was excited with the 266 nm laser sheet, and detected via the ICCD camera between 350 and 400 nm. For gaps of 2.25 cm, 1.5 cm, and 1.0 cm, fluorescence collection problems were minor; the  $\text{CF}_2$  density within 0.5 mm of the upper electrode and 1 mm to 2 mm of the lower electrode surfaces may be reduced due to shadowing of the electrodes. Because errors were so small and dividing by the acetone images introduces noise, the  $\text{CF}_2$  PLIF images for these gaps were not corrected. For the case of the smallest gap (0.5 cm), the acetone PLIF images indicated that corrections to the  $\text{CF}_2$  fluorescence intensity of up to 25% were necessary. Thus, the images for the 0.5 cm gap were divided by the normalized acetone images. The application of this correction introduces up to an estimated additional  $\pm 10\%$  error on the overall magnitude of the 0.5 cm gap PLIF intensity.

### III. RESULTS AND DISCUSSION

#### A. Planar laser-induced fluorescence results

$\text{CF}_2$  PLIF results at selected pressures are shown in Figs. 2, 3, 4, and 5 for electrode gaps of 2.25 cm, 1.5 cm, 1.0 cm, and 0.5 cm, respectively. Each image shows a vertical cross section through half of the plasma, with the radial center of the reactor located on the left-hand side and the outer edge of the electrodes located on the right-hand side. Bold lines near the top and bottom of each image indicate the outlines of the upper and lower electrodes and the insulator and ground shield of the upper electrode. PLIF measurements of the  $\text{CF}_2$  density are plotted using contour lines. All PLIF contour values in Figs. 2, 3, 4, and 5 are normalized to the same intensity scale (in arbitrary units).

In Fig. 2, the full electrode gap of 2.25 cm is shown for 53 Pa (400 mTorr), 93 Pa (700 mTorr), and 133 Pa (1000 mTorr). In this case, no disks were necessary to narrow the gap, and the only difference between these images and previous results<sup>1</sup> is that the upper electrode is now powered instead of the lower electrode. As discussed previously,<sup>1</sup> three types of behavior are observed. At low pressures, as shown in Fig. 2(a), the  $\text{CF}_2$  density has a broad peak near the edge of the powered electrode. At intermediate pressures as in Fig. 2(b), the  $\text{CF}_2$  density is more confined to the region between the electrodes, is more radially uniform, and its value at the radial center is higher than at lower pressures. At high pressures such as in Fig. 2(c), however, the  $\text{CF}_2$  intensity near the radial center decreases with pressure, and a very sharp maximum in  $\text{CF}_2$  appears near the edge of the powered electrode. The different behaviors seen at different pressures in Fig. 2 are largely caused by changes in how and where  $\text{CF}_2$  is created in the discharge.<sup>1</sup> Such changes are correlated to and explained by optical emission and electrical measurements, which will be discussed in detail in Secs. III B and III C below.

The  $\text{CF}_2$  PLIF images shown in Fig. 3 for an electrode gap of 1.5 cm are similar to those for the 2.25 cm gap. At the

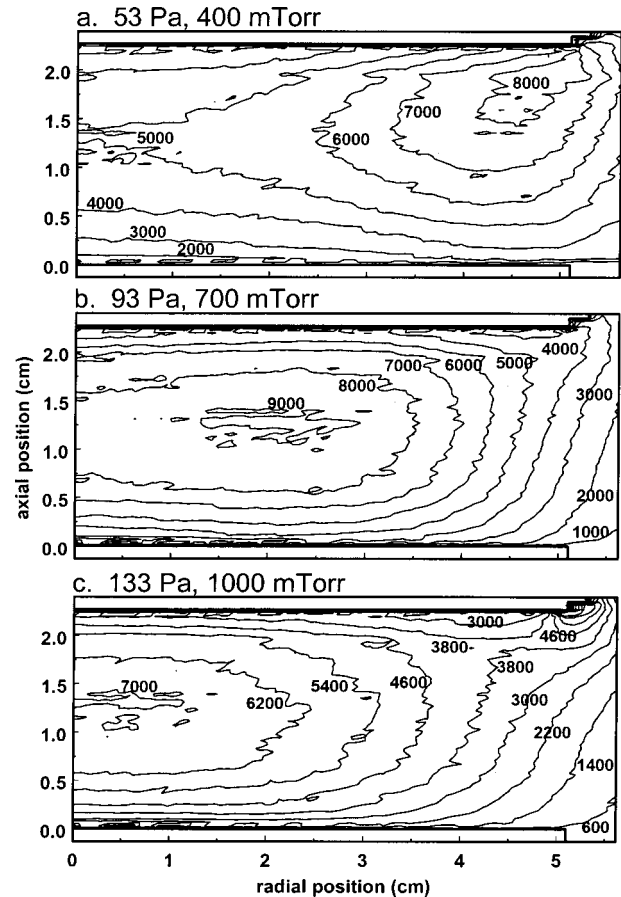


Fig. 2.  $\text{CF}_2$  PLIF contour maps in a 30 W, 9%  $\text{O}_2/91\%$   $\text{CF}_4$  plasma with a gap of 2.25 cm at pressures of (a) 53 Pa (400 mTorr), (b) 93 Pa (700 mTorr), and (c) 133 Pa (1000 mTorr). Outlines of the upper (powered) and lower (grounded) electrodes are shown. Each contour map displays half of the plasma, such that the left-hand side of the map shows the plasma center and the right-hand side shows the electrode edge. All PLIF contour values in Figs. 2, 3, 4, and 5 are normalized to the same intensity scale (in arbitrary units).

lowest pressure, 27 Pa (200 mTorr), shown in Fig. 3(a), the  $\text{CF}_2$  distribution is quite similar to that of Fig. 2(a). Furthermore, as the pressure in Fig. 3 increases, the maximum of  $\text{CF}_2$  density moves radially inward, the distribution becomes more radially uniform, and the  $\text{CF}_2$  density at the radial center increases, as in Fig. 2(b). In Fig. 3, however, the highest values of  $\text{CF}_2$  density at the radial center and the maximum radial uniformity occur at 107 Pa (800 mTorr), whereas in Fig. 2 they occur at 93 Pa (700 mTorr). At 133 Pa (1000 mTorr), in Fig. 3(e), the  $\text{CF}_2$  density in the center of the plasma decreases slightly, but, unlike Fig. 2(c), no maximum in the  $\text{CF}_2$  density is observed near the edge of the powered electrode. In this respect, the effect of narrowing the gap from 2.25 to 1.5 cm is similar to that observed when the rf power is increased or the gas mixture is made less electronegative. Any of these changes will act to prevent the formation of the sharp maximum in  $\text{CF}_2$  density near the electrode edge, or postpone its formation to higher pressures.<sup>1</sup>

In Fig. 4, the  $\text{CF}_2$  density maps for the 1.0 cm gap show a similar trend; the peak in  $\text{CF}_2$  density at the center of the plasma and the maximum radial uniformity occur at a still

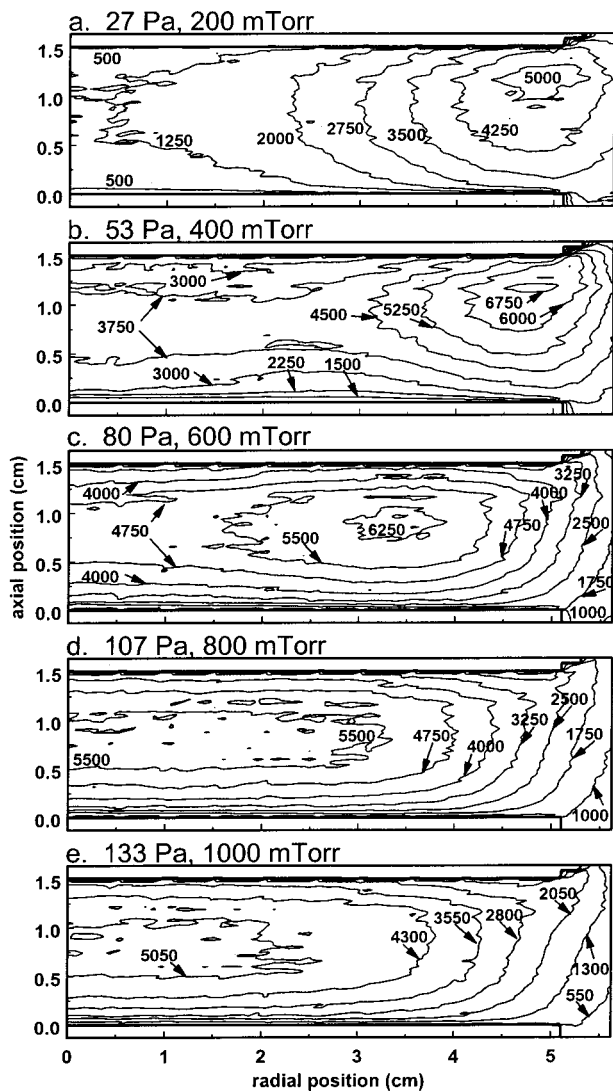


Fig. 3.  $\text{CF}_2$  PLIF contour maps in a 30 W, 9%  $\text{O}_2/\text{CF}_4$  plasma with a gap of 1.5 cm at pressures of (a) 27 Pa (200 mTorr), (b) 53 Pa (400 mTorr), (c) 80 Pa (600 mTorr), (d) 107 Pa (800 mTorr), and (e) 133 Pa (1000 mTorr).

higher pressure of 120 Pa (900 mTorr), shown in Fig. 4(e). At high pressures, no maximum in  $\text{CF}_2$  density near the electrode edge is observed. Indeed, in Fig. 4, there is very little change between 107 Pa (800 mTorr) and 133 Pa (1000 mTorr), as shown in Figs. 4(d)–4(f). Thus, narrowing the electrode gap from 2.25 cm to 1.0 cm causes the plasma to be less sensitive to changes in pressure, for pressures in this range.

The  $\text{CF}_2$  PLIF images for the 0.5 cm electrode gap, shown in Fig. 5, display somewhat different behavior than the data for previous gaps. At the lower pressures of 40 Pa and 53 Pa (300 mTorr and 400 mTorr), as show in Figs. 5(a) and 5(b), the  $\text{CF}_2$  density does show a maximum near the outer edge of the powered electrode, similar to the previous gaps. However, for this gap, the spatial distribution of  $\text{CF}_2$  remains very similar in the bulk of the plasma for the entire pressure range from 53 to 133 Pa (400 to 1000 mTorr). In this region, the  $\text{CF}_2$  density is fairly radially uniform, but not as uniform as was observed for previous gaps, and the  $\text{CF}_2$  also shows a

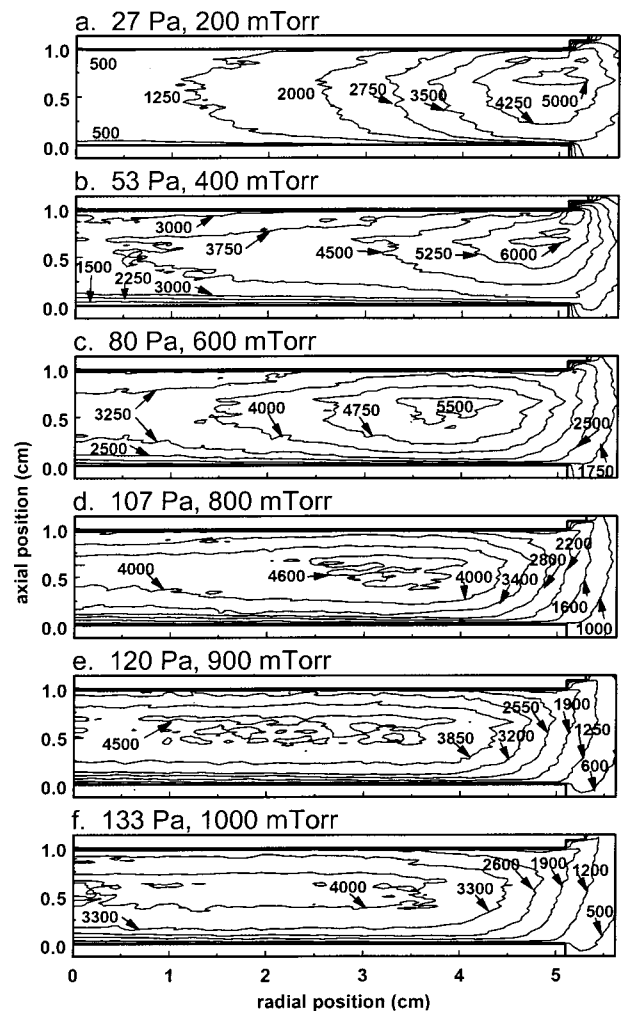


Fig. 4.  $\text{CF}_2$  PLIF contour maps in a 30 W, 9%  $\text{O}_2/\text{CF}_4$  plasma with a gap of 1.0 cm at pressures of (a) 27 Pa (200 mTorr), (b) 53 Pa (400 mTorr), (c) 80 Pa (600 mTorr), (d) 107 Pa (800 mTorr), (e) 120 Pa (900 mTorr), and (f) 133 Pa (1000 mTorr).

small decrease in density with increasing pressure.

In all of the images, we observe a decreasing gradient of  $\text{CF}_2$  density near the electrode surfaces. This indicates that the electrode surfaces act as a sink for  $\text{CF}_2$ . Additional evidence for the surface loss of  $\text{CF}_2$  will be given next in Sec. III C.

## B. Broadband optical emission

Whereas the  $\text{CF}_2$  PLIF measurements detect  $\text{CF}_2$  in its electronic ground state, the emission images indicate where hot electrons create electronically excited atoms and radicals, including  $\text{CF}_2$ , as discussed in Sec. I. Care must be taken when interpreting the emission images, which (unlike the PLIF images) are line-of-sight integrated. The camera is focused on a vertical plane which slices through the middle of the plasma, but emission is also collected both in front of and behind this plane. Thus, in Figs. 6 and 7, the emission at  $R = 0$  is not necessarily from the radial center; rather, it includes contributions from other radii along the line of sight.

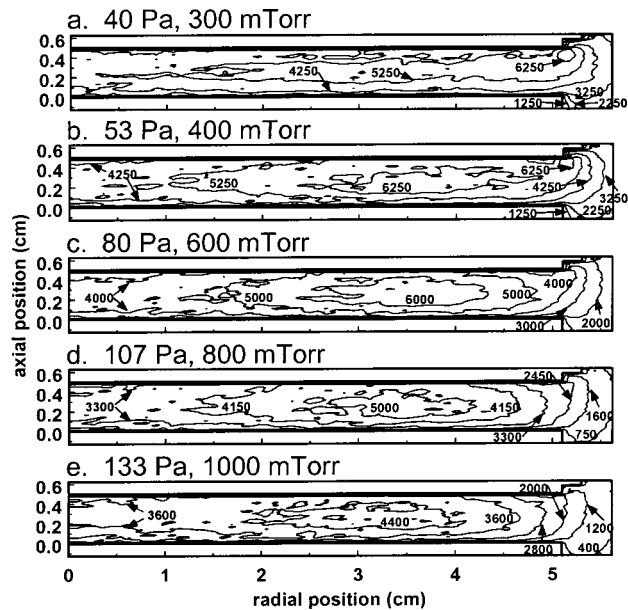


Fig. 5.  $\text{CF}_2$  PLIF contour maps in a 30 W, 9%  $\text{O}_2/\text{CF}_4$  plasma with a gap of 0.5 cm at pressures of (a) 40 Pa (300 mTorr), (b) 53 Pa (400 mTorr), (c) 80 Pa (600 mTorr), (d) 107 Pa (800 mTorr), and (e) 133 Pa (1000 mTorr).

This effect, discussed further in Ref. 1, does not, however, alter any of the conclusions made about the emission data presented next.

Figure 6 shows contour maps of broadband optical emission intensity (collected from 300 to 400 nm) at 53 Pa (400 mTorr) as a function of pressure, for the full electrode gap of 2.25 cm. The results are similar to a previous study<sup>1</sup> except that, here, the upper electrode is powered, not the lower. For all pressures, emission occurs primarily near the powered upper electrode and the lower grounded electrode, with less emission occurring in the bulk regions. At 53 Pa (400 mTorr), the maximum emission intensity is observed near the edge of the upper electrode. At 93 Pa (700 mTorr), a long narrow region of high emission intensity is observed along nearly the whole length of the upper electrode, and an additional maximum is observed at the radial center of the lower electrode. At 133 Pa (1 Torr), three maxima are observed: At the edge and center of the upper electrode as well as the center of the lower electrode.

$\text{CF}_2$  created predominantly in the regions of high emission intensity seen in Fig. 6 diffuses some distance away, producing the  $\text{CF}_2$  distributions shown in Fig. 2. At 53 Pa (400 mTorr),  $\text{CF}_2$  generated near the edge of the upper electrode diffuses several centimeters away, forming the toroidal-shaped distribution of Fig. 2(a). At 93 Pa (700 mTorr),  $\text{CF}_2$  generated over a broad range of radii and near either electrode diffuses into the gap to form the distribution of Fig. 2(b), which is rather uniform in the radial and axial directions. As can also be seen in Fig. 2(b), the  $\text{CF}_2$  decreases near the electrode surfaces, indicating that surface reactions form an important loss mechanism for  $\text{CF}_2$  under these conditions. At 133 Pa (1 Torr),  $\text{CF}_2$  is not able to diffuse as far as at lower pressures, so the  $\text{CF}_2$  generated near both the edge and the center of the electrodes form two separate regions of

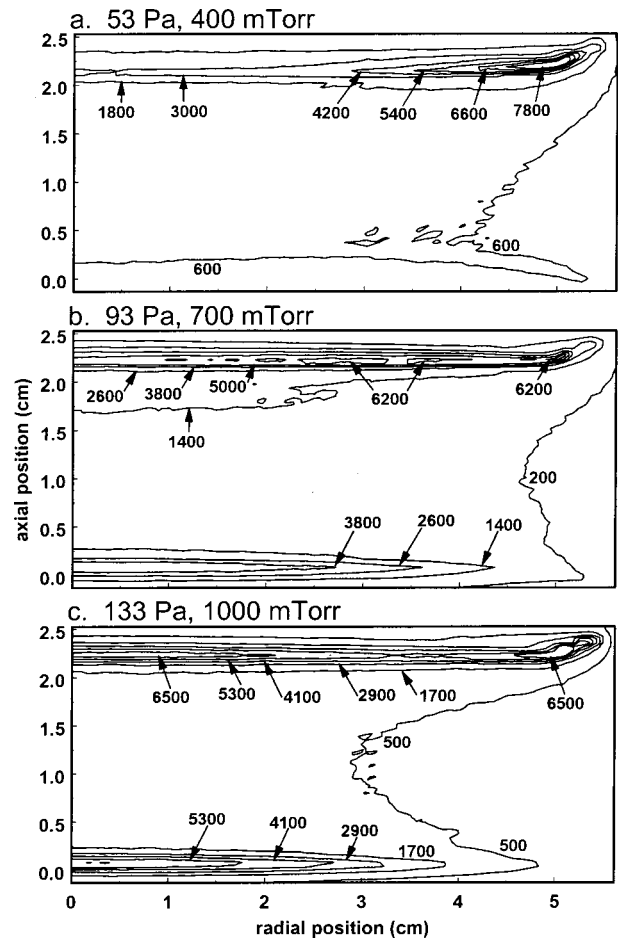


Fig. 6. Broadband emission contour maps in a 30 W, 9%  $\text{O}_2/\text{CF}_4$  plasma with a gap of 2.25 cm at pressures of (a) 53 Pa (400 mTorr), (b) 93 Pa (700 mTorr), and (c) 133 Pa (1000 mTorr). The electrodes are not shown. The lower electrode is at axial position = 0 cm, and the upper electrode is at axial position = 2.25 cm. All emission contour values in Figs. 6 and 7 are normalized to the same intensity scale (in arbitrary units, independent of the PLIF intensity scale).

high  $\text{CF}_2$  density, shown in Fig. 2(c), rather than merging into a single region.

Figure 7 shows emission results from the 1.0 cm gap. The results are very similar to Fig. 6, except that, at 133 Pa (1 Torr), the strong emission maximum near the edge of the powered electrode in Fig. 6(c) does not appear in Fig. 7(c). Emission results from the 1.5 cm and 0.5 cm gaps were similar—they also showed no maximum near the electrode edge at 133 Pa (1 Torr). The elimination of the emission feature implies that much less  $\text{CF}_2$  is created near the edge of the powered electrode. Consequently, less  $\text{CF}_2$  is observed near the electrode edge in Figs. 3(e), 4(f), and 5(e), compared to Fig. 2(c). A mechanism that explains how the smaller gaps eliminate this edge emission at high pressures is given next in Sec. III C.

### C. rf current measurements

In previous studies in the GEC reference cell, PLIF, and optical emission results were found to be correlated with electrical measurements.<sup>1,2,20,21</sup> Measurements of the rf cur-

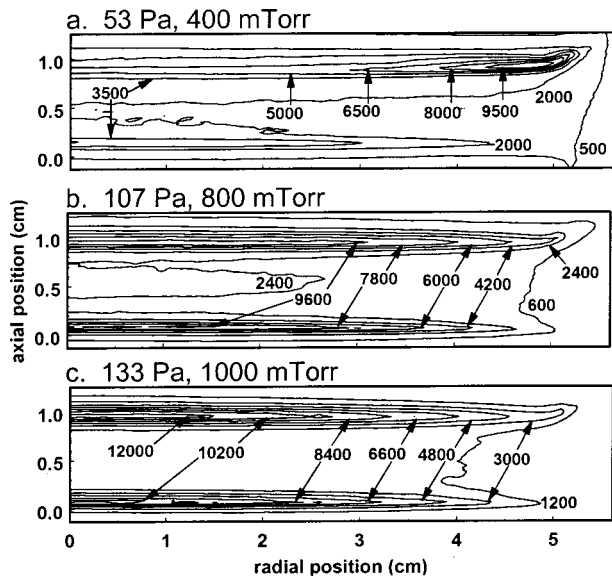


FIG. 7. Broadband emission contour maps in a 30 W, 9%  $O_2/CF_4$  plasma with a gap of 1.0 cm at pressures of (a) 53 Pa (400 mTorr), (b) 107 Pa (800 mTorr), (c) 133 Pa (1000 mTorr). The electrodes are not shown. The lower electrode is at axial position=0 cm, and the upper electrode is at axial position=1.0 cm.

rent were particularly closely correlated. Such correlations can be explained as follows. The rf current flowing from the powered electrode into the plasma can flow out of the plasma by several different paths. It may flow directly across the gap to the grounded electrode or it may flow radially outward to the ground shield of either electrode or to the wall of the vacuum chamber. If the path taken by the rf current changes, the locations in the discharge where rf power is absorbed will also change. Electrons are heated by the rf power, and some of them gain enough energy to exceed the thresholds for electron impact dissociation and electronic excitation. The spatial distribution of the energetic electrons, and of species produced by collisions with these electrons, will therefore vary depending on the path taken by the rf current.

To quantify the relative importance of different current paths, we use the parameter  $|I_{ge}|/|I_{pe}|$ , the ratio of the fundamental (i.e., 13.56 MHz) magnitudes of the current at the grounded and powered electrodes. As shown in Fig. 8(a),  $|I_{ge}|/|I_{pe}|$  varies widely with conditions, ranging from 0.34 to 0.96. In other words, 34% to 96% of the total current flows directly across the gap between the two electrodes, with the remainder of the current flowing outward to the ground shields of either electrode or the vacuum chamber wall. As might be expected,  $|I_{ge}|/|I_{pe}|$  increases with decreasing gap: The current path directly from one electrode to the other becomes more favorable to current flow as the gap between them becomes shorter. The length of each current path is not the only consideration, however. The current flow between two surfaces will depend on their surface areas as well as their separation. Thus, the current path from the edge of the powered electrode directly to its ground shield is very short, but it also has a relatively small surface area associated with it, so it will not necessarily be the dominant path.

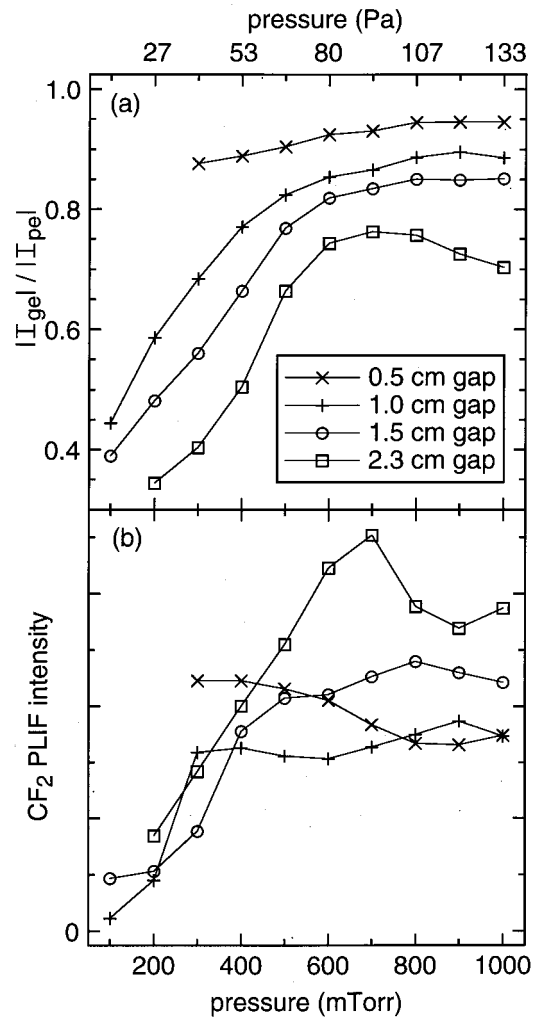


FIG. 8. Plots vs pressure for (a)  $I_{ge}/I_{pe}$ , the ratio of the fundamental (13.56 MHz) amplitudes of the current at the ground electrode and the powered electrode. The uncertainty in  $I_{ge}/I_{pe}$ , obtained by propagating the measurement uncertainty of the oscilloscope and its probes, is  $\pm 0.04$ . (b)  $CF_2$  PLIF integrated axially between the electrode surfaces and radially from 0.0 cm to 0.2 cm. Uncertainty in the PLIF measurements are discussed in Sec. II.

The lowest values of  $|I_{ge}|/|I_{pe}|$  are observed at the lowest pressures. At such pressures, the plasma is not confined to the gap between the electrodes; it extends out toward the chamber wall. Consequently, a large fraction of the rf current can flow out to remote surfaces, and only a relatively small fraction flows to the grounded electrode, because under these conditions where impedance is dominated by the capacitive impedance of the sheath, discussed below in Sec. III D, the magnitude of the current flow to a surface is proportional to the surface area. As the pressure increases up to around 93 Pa (700 mTorr), the bulk plasma resistive impedance increases and reduces current flow to the more remote surfaces, and the plasma becomes more confined to the gap between the electrodes. Consequently,  $|I_{ge}|/|I_{pe}|$  increases with pressure in this range. For the full gap (2.25 cm)  $|I_{ge}|/|I_{pe}|$  reaches a maximum at 93 Pa (700 mTorr) and then starts to decline with pressure. Presumably, as the pressure increases above 93 Pa (700 mTorr), the bulk plasma resistive impedance

dominates, and an increasing fraction of the rf current takes the very short path from the edge of the powered electrode directly to its ground shield, giving rise to the maxima in optical emission intensity and  $\text{CF}_2$  density observed in that vicinity in Figs. 2(c) and 6(c). In contrast, for the three smaller gaps,  $|I_{\text{ge}}|/|I_{\text{pe}}|$  is more or less constant above 93 Pa (700 mTorr), ranging from roughly 85% for the 1.5 cm gap to 95% for the 0.5 cm gap. Apparently, by making the gap less than 2.25 cm, we prevent current from taking the very short path from the edge of the powered electrode to its ground shield. Consequently, the maxima in emission intensity and  $\text{CF}_2$  density near the electrode edge in Figs. 2(c) and 6(c) are not observed for the 0.5 cm to 1.5 cm gaps.

For comparison with  $|I_{\text{ge}}|/|I_{\text{pe}}|$ , the  $\text{CF}_2$  PLIF intensity has been integrated axially between the electrode surfaces and radially from 0.0 to 0.2 cm for each image and is plotted versus pressure in Fig. 8(b). At low pressures, the  $\text{CF}_2$  density at the radial center increases with pressure, similar to  $|I_{\text{ge}}|/|I_{\text{pe}}|$ . This is presumably due to an increase in the generation of  $\text{CF}_2$  at the radial center which accompanies the increase in  $|I_{\text{ge}}|/|I_{\text{pe}}|$ . The pressure dependence at high pressures is also similar in Figs. 8(a) and 8(b). For the 2.25 cm gap, both  $|I_{\text{ge}}|/|I_{\text{pe}}|$  and the  $\text{CF}_2$  at the radial center decrease when the pressure is increased above 93 Pa (700 mTorr). For the other gaps, both  $|I_{\text{ge}}|/|I_{\text{pe}}|$  and the  $\text{CF}_2$  at the radial center are relatively independent of pressure. The dependence on electrode gap, however, differs in Figs. 8(a) and 8(b). Unlike  $|I_{\text{ge}}|/|I_{\text{pe}}|$ , which increases with decreasing gap, the  $\text{CF}_2$  at the radial center generally decreases as the gap is narrowed, except at the lower pressures for the smallest gaps. This decrease is consistent with the electrode surfaces acting as sink for  $\text{CF}_2$ ; as the gap decreases from 2.25 to 0.5 cm, the ratio of the area of the electrodes to the volume of the gap increases by a factor of 4.5, which should greatly increase the importance of surface losses. The  $\text{CF}_2$  density depends on the mechanisms by which it is destroyed as well as the mechanisms by which it is created, whereas  $|I_{\text{ge}}|/|I_{\text{pe}}|$  is closely correlated to the latter mechanisms, but not the former.

#### D. Electrical impedance analysis

A better understanding of why  $|I_{\text{ge}}|/|I_{\text{pe}}|$  behaves as it does in Fig. 8(a) can be obtained by considering the electrical impedance of the different current paths through the discharge. The impedance of the current path that passes directly from the powered electrode through the gap to the grounded electrode is

$$Z_{\text{gap}} = V_{\text{pe}}/I_{\text{ge}}, \quad (1)$$

where  $V_{\text{pe}}$  is the fundamental component of the voltage at the powered electrode. Current paths that pass from the powered electrode to all other surfaces, e.g., to the chamber wall or either ground shield, have a combined impedance

$$Z_{\text{edge}} = V_{\text{pe}}/(I_{\text{pe}} - I_{\text{ge}}). \quad (2)$$

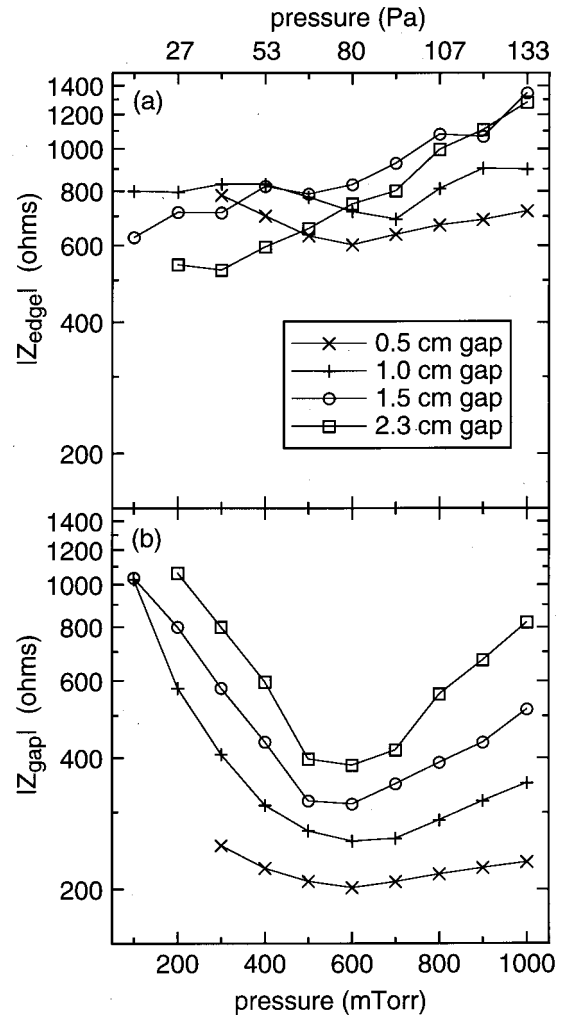


Fig. 9. Plots vs pressure for the magnitude of (a) the combined impedance of the current paths that pass from the powered electrode to all surfaces other than the grounded electrode,  $|Z_{\text{edge}}|$ , and (b) the impedance of the current path that passes directly from the powered electrode through the gap to the grounded electrode,  $|Z_{\text{gap}}|$ . The uncertainty obtained by propagating the measurement uncertainty of the oscilloscope and its probes, is typically  $\pm 10\%$  for  $Z_{\text{gap}}$  and  $\pm 15\%$  for  $Z_{\text{edge}}$ .

Because  $Z_{\text{gap}}$  and  $Z_{\text{edge}}$  are in parallel, their combined impedance,  $(Z_{\text{gap}}^{-1} + Z_{\text{edge}}^{-1})^{-1}$ , will be dominated by whichever is smaller. A decrease in  $Z_{\text{gap}}$  relative to  $Z_{\text{edge}}$  forces more current to flow across the gap.

The magnitudes of  $Z_{\text{gap}}$  and  $Z_{\text{edge}}$ ,  $|Z_{\text{gap}}|$  and  $|Z_{\text{edge}}|$ , are plotted in Fig. 9. In Fig. 9(a),  $|Z_{\text{edge}}|$  is seen to be relatively insensitive to pressure and electrode gap. In contrast, in Fig. 9(b),  $|Z_{\text{gap}}|$  shows a strong dependence on pressure and gap. As might be expected,  $|Z_{\text{gap}}|$  is smaller for smaller gaps. The pressure dependence is more complicated. Starting at low pressures,  $|Z_{\text{gap}}|$  falls with pressure, reaches a minimum near 80 Pa (600 mTorr) and then increases with pressure. These changes in  $|Z_{\text{gap}}|$  are mirrored in the  $|I_{\text{ge}}|/|I_{\text{pe}}|$  data in Fig. 8(a). The decrease in  $|Z_{\text{gap}}|$  from 13 Pa to 80 Pa (100 to 600 mTorr) coincides with an increase in  $|I_{\text{ge}}|/|I_{\text{pe}}|$ . The rapid increase in  $|Z_{\text{gap}}|$  from 80 to 133 Pa (600 to 1000 mTorr) for the 2.25 cm gap coincides with a decrease in  $|I_{\text{ge}}|/|I_{\text{pe}}|$ . The decrease in  $|Z_{\text{gap}}|$  for decreasing electrode gap coincides with

an increase in  $|I_{ge}|/|I_{pe}|$ . Thus, for the conditions studied here, changes in  $|I_{ge}|/|I_{pe}|$  are determined primarily by changes in the gap impedance, rather than the edge impedance.

The complicated pressure dependence of  $Z_{gap}$  arises because it is the sum of two components: A largely resistive impedance associated with the plasma itself in series with a largely capacitive impedance contributed by the plasma sheaths. Although in general, the sheaths may also contribute a resistance<sup>15,22,23</sup> and the plasma may also contribute capacitive and inductive impedances,<sup>21</sup> the effects of these elements are usually quite minor. If these minor elements are neglected, the resistive impedance of the plasma and the capacitive impedance of the sheath can be obtained directly as the real and imaginary parts of  $Z_{gap}$ , respectively:

$$\text{Re}(Z_{gap}) = |Z_{gap}| \cos \phi_{gap}, \quad (3)$$

and

$$\text{Im}(Z_{gap}) = |Z_{gap}| \sin \phi_{gap}, \quad (4)$$

where  $\phi_{gap}$  is the phase of  $Z_{gap}$ , i.e., the phase of  $V_{pe}$  relative to  $I_{ge}$ .

Values of  $\text{Re}(Z_{gap})$  and  $\text{Im}(Z_{gap})$  are shown in Fig. 10(a). There,  $\text{Re}(Z_{gap})$  is positive, and it increases with increasing pressure and larger electrode gaps. In contrast,  $\text{Im}(Z_{gap})$  is negative, which indicates that the sheath impedance is indeed capacitive rather than inductive. Starting at low pressures,  $\text{Im}(Z_{gap})$  becomes less negative with increasing pressure, and then it becomes pressure independent. Because the plasma impedance and sheath impedance are in series, the magnitude of the total impedance,

$$|Z_{gap}| = \{[\text{Re}(Z_{gap})]^2 + [\text{Im}(Z_{gap})]^2\}^{1/2}, \quad (5)$$

will be dominated by whichever has the larger magnitude. At low pressures,  $|\text{Im}(Z_{gap})| \gg |\text{Re}(Z_{gap})|$ , so the capacitive impedance is dominant,  $|Z_{gap}| \approx -\text{Im}(Z_{gap})$ , and  $|Z_{gap}|$  therefore decreases with pressure. In contrast, at high pressures (and large gaps),  $|\text{Re}(Z_{gap})| \gg |\text{Im}(Z_{gap})|$ , so the resistive impedance is dominant,  $|Z_{gap}| \approx \text{Re}(Z_{gap})$ , and  $|Z_{gap}|$  therefore increases with pressure. The minimum in  $|Z_{gap}|$  occurs at intermediate pressures, around 80 Pa (600 mTorr), where  $\text{Re}(Z_{gap})$  and  $\text{Im}(Z_{gap})$  have comparable magnitudes.

Many features of the plots in Fig. 10(a) are predicted by simple models of the plasma resistance and sheath impedance. For example, if one assumes that a uniform plasma of electron density  $n_e$  and electron collision frequency  $\nu_e$  fills the entire gap between the electrodes, one obtains a plasma resistance<sup>21</sup>

$$R_p = m_e \nu_e L / (n_e e^2 A), \quad (6)$$

where  $m_e$  and  $e$  are the mass and charge of an electron,  $L$  is the electrode gap, and  $A$  is the electrode area. Because  $\nu_e$  is directly proportional to pressure, Eq. (6) predicts that (at constant  $n_e$ ) the plasma resistance should vary linearly with pressure and with gap. In agreement with this prediction, measured values of  $\text{Re}(Z_{gap})$  at high pressures in Fig. 10(a) are indeed roughly proportional to pressure and gap. The gap

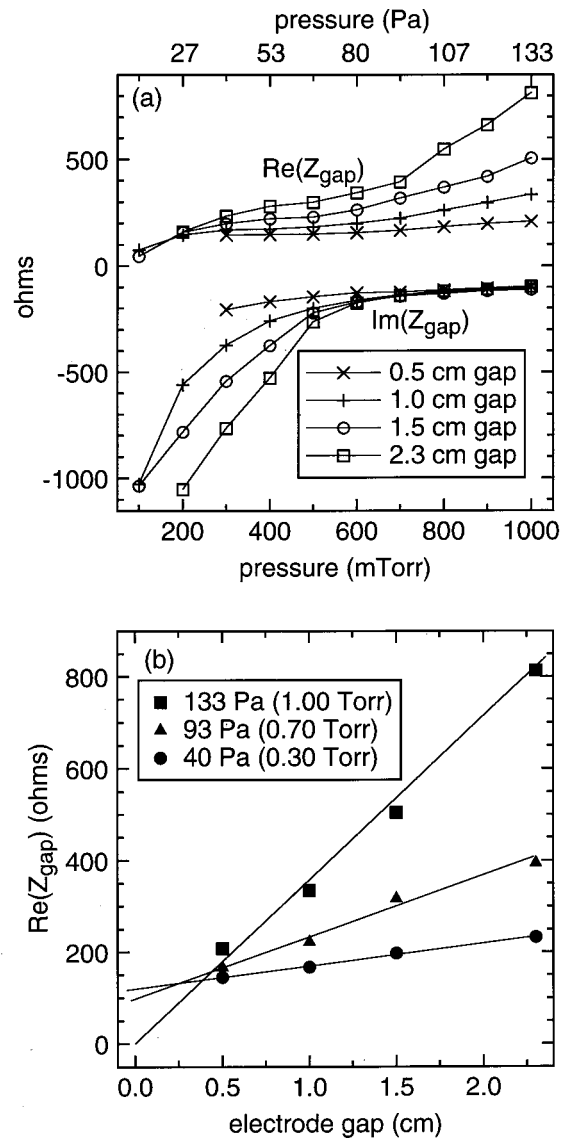


FIG. 10. (a) The real and imaginary parts of the gap impedance,  $\text{Re}(Z_{gap})$  and  $\text{Im}(Z_{gap})$  vs pressure and (b)  $\text{Re}(Z_{gap})$  vs gap,  $L$ . The uncertainty in  $\text{Re}(Z_{gap})$  and  $\text{Im}(Z_{gap})$  obtained by propagating the measurement uncertainty of the oscilloscope and its probes, is  $\pm 12\%$ .

dependence is better illustrated in Fig. 10(b), which plots measurements of  $\text{Re}(Z_{gap})$  directly versus gap.

The predicted linear dependences on pressure and gap are only valid if the electron density  $n_e$  is independent of pressure and gap. Although the total power delivered to the discharge is held constant for all gaps and pressures, at lower pressures, a significant fraction of the power is absorbed by ions in the sheaths.<sup>15,21,22,24</sup> Thus, the power absorbed by electrons, which sustains the plasma, decreases at lower pressures, and presumably  $n_e$  decreases as well. A decrease in  $n_e$  with decreasing pressure would partially counteract the effect of  $\nu_e$  in Eq. (6) resulting in a weaker than linear pressure dependence, as is indeed observed in the plots of  $\text{Re}(Z_{gap})$  at low pressures in Fig. 10(a).

Like  $\text{Re}(Z_{gap})$ , the behavior of  $\text{Im}(Z_{gap})$  in Fig. 10(a) can also be explained using models. Modeling the capacitive im-

pedance of plasma sheaths is, however, more complicated than modeling the plasma resistance. Many different sheath models have been proposed, and further development and testing of these models remains an area of active research. Here, we use a simple, analytic model derived by Lieberman.<sup>25</sup> For high frequencies and high sheath voltages, and at pressures low enough that ion collisions in the sheath can be ignored, Lieberman calculates a sheath impedance,  $Z_s$ , that can be expressed as

$$Z_s = -0.76i(e/m_i)^{1/4}(\epsilon_0/J_i)^{1/2}V_s^{3/4}(\omega\epsilon_0A)^{-1}, \quad (7)$$

where  $m_i$  is the ion mass,  $\epsilon_0$  is the permittivity of vacuum,  $J_i$  is the ion current density,  $V_s$  is the fundamental component of the sheath voltage,  $\omega = 2\pi f$ , and  $f$  is the rf frequency.

According to Eq. (7), the sheath capacitance has a strong dependence on the sheath voltage, and it is this dependence that gives rise to the behavior of  $\text{Im}(Z_{\text{gap}})$  in Fig. 10(a). At low pressures, the fundamental voltage on the powered electrode,  $V_{\text{pe}}$ , is large [280 to 340 V at 13 Pa (100 mTorr)]. Because the plasma resistance at low pressures is small, nearly all of  $V_{\text{pe}}$  is dropped across the sheaths, rather than across the plasma. Indeed, the combined voltage across both sheaths, given by  $V_{\text{pe}} \sin \phi_{\text{gap}}$ , is 270 to 340 V at 13 Pa (100 mTorr), comparable to  $V_{\text{pe}}$ . The dc bias on the powered electrode,  $V_0$ , is also large at low pressures [ranging from  $-140$  to  $-180$  V at 13 Pa (100 mTorr)], which is another sign that large sheath voltages are present, and which further indicates that the voltage is divided unequally, with a larger voltage drop occurring across the sheath at the powered electrode.

As the pressure increases, however, the total voltage,  $V_{\text{pe}}$ , decreases and, because the plasma resistance increases, the voltage drop across the plasma, given by  $V_{\text{pe}} \cos \phi_{\text{gap}}$ , increases. Both of these effects reduce the voltage drop across the sheaths. According to Eq. (7), the reduction in sheath voltage accompanies a decrease in the magnitude of the sheath impedance, as is observed for  $\text{Im}(Z_{\text{gap}})$  in Fig. 10(a). The decrease in sheath impedance, in turn, forces a greater fraction of the voltage to be dropped across the plasma which further decreases the sheath voltage and sheath impedance. Thus, the nonlinearity present in Eq. (7) (i.e., its voltage dependence) provides a sort of positive feedback, making the reduction in sheath voltage with pressure more rapid than it would be if the sheath impedance did not depend on sheath voltage. At 133 Pa (1000 mTorr), the voltage drop across the plasma is 110 to 200 V, comparable to the applied voltage,  $V_{\text{pe}}$ , but the rf voltage across the sheaths, given by  $V_{\text{pe}} \sin \phi_{\text{gap}}$ , is only 20 to 60 V, and the dc bias is only  $-5$  to  $-20$  V. These low sheath voltages at high pressures result in a low sheath impedance, which is also rather independent of gap and pressure.

In addition to providing qualitative explanations for our experimental results, from the simple analysis of plasma resistance and sheath impedance presented here, we were also able to make some useful predictions. For example, Eq. (6) predicts that, if one raises the pressure (and, hence  $\nu_e$ ) high enough, high values of the plasma resistance,  $R_p$ , can be obtained even for small values of  $L$ . Eventually,  $R_p$  should

become comparable to the edge impedance, causing a shift in rf current, optical emission, and  $\text{CF}_2$  density to the powered ground shield of the electrode. Measurements made above 133 Pa (1.0 Torr) for the 0.5 cm gap confirm this prediction. We observed that  $|I_{\text{ge}}|/|I_{\text{pe}}|$  peaked at a value of 0.9 at 187 Pa (1.4 Torr) and declined to 0.7 at 267 Pa (2.0 Torr). At the same time as the decline in  $|I_{\text{ge}}|/|I_{\text{pe}}|$ , a decrease in optical emission near the radial center of the plasma and an increase near the powered electrode ground shields was observed visually. Similarly, if one increases the power delivered to the discharge, thereby increasing  $n_e$ , the plasma resistance in Eq. (6) should be reduced, causing the same effect on  $|I_{\text{ge}}|/|I_{\text{pe}}|$  as that produced by a decrease in  $L$ . This prediction was also confirmed. When we increased the delivered power from 30 to 100 W, the peak in  $|I_{\text{ge}}|/|I_{\text{pe}}|$  shifted from 93 (700 mTorr) to 160 Pa (1.2 Torr). Decreasing the delivered power to 10 W shifted the peak in  $|I_{\text{ge}}|/|I_{\text{pe}}|$  down to 53 Pa (400 mTorr). Finally, using a more electronegative gas mixture should decrease  $n_e$ , and thus act in the same manner as a decrease in discharge power. As predicted, in more electronegative mixtures of  $\text{C}_2\text{F}_6/\text{O}_2$ , we observed the peak in  $|I_{\text{ge}}|/|I_{\text{pe}}|$  to occur at pressures of 13 to 27 Pa (100 to 200 mTorr), which are below that of the  $\text{CF}_4/\text{O}_2$  mixtures studied here. Thus, qualitative predictions for the effect of electrode gap, power, and electronegativity are all obtained easily from Eq. (6). To obtain accurate quantitative predictions for these effects would however require a great deal of additional modeling, and perhaps additional measurements as well. Measurements of the electron density,  $n_e$ , for each experimental condition would greatly assist in the selection, development and validation of the models.

The results and analysis presented here have several implications for chamber-cleaning processes. Previous studies<sup>26</sup> have shown that chamber cleaning of surfaces at the radial center of a reactor often operate efficiently only over a narrow range of pressures. At low pressures, where the sheath impedance is dominant and sheath voltages are large, a large fraction of the delivered rf power is absorbed by ions in the plasma sheaths.<sup>21</sup> For chamber cleaning—and any other processes that are purely chemical—the power absorbed by ions is wasted. Furthermore, the energetic ions produced at low pressures can damage reactor surfaces. On the other hand, if the pressure is too high, the resistance of the plasma in the gap between the electrodes can exceed the impedance of more remote current paths. In the GEC cell, as discussed herein, this causes the plasma to move out from the radial center toward the powered electrode ground shield. In commercial reactors, the same effect causes the plasma to retreat out of the electrode gap toward more remote surfaces. Such conditions lead to poor gas utilization efficiency.<sup>27</sup> Processes intended to clean the electrode surfaces may therefore benefit from narrowing the electrode gap, since this reduces the plasma resistance, thus retarding the retreat of the plasma to remote surfaces, maintaining a high plasma density near the radial center of the reactor, and extending the operating range to higher pressures. Narrowing the gap may also be beneficial if good radial uniformity of plasma chemical spe-

cies is desired at high pressures. At low pressures, where the sheath impedance is dominant, narrowing the gap does not much affect the radial uniformity, but one may control the uniformity using an alternative technique<sup>2,20</sup> in which external inductive impedances cancel out sheath impedances. At high pressures, where the plasma resistance dominates, the uniformity becomes insensitive to external impedances, but it is sensitive to the electrode gap.

#### IV. CONCLUSIONS

In this study, PLIF has been utilized to measure the spatial distribution of CF<sub>2</sub> as a function of electrode gap in 30 W, 9% O<sub>2</sub>/91% CF<sub>4</sub> chamber-cleaning plasmas. Together with plasma current and voltage measurements, these data provide valuable insight into these plasmas. At low pressures, independent of the size of the gap, a broad maximum in CF<sub>2</sub> density is observed near the outer edge of the electrodes. As the pressure is increased to intermediate values, the CF<sub>2</sub> density and optical emission intensity become more radially uniform for all the gaps, and the CF<sub>2</sub> density at the radial center of the reactor increases for all but the smallest gap. For the largest gap, as the pressure is further increased, these trends reverse, and the CF<sub>2</sub> density and optical emission intensity become less uniform radially, and they both show sharp strong maxima located between the outer edge of the powered electrode and its ground shield. Smaller gaps, however, prevent the formation of the sharp maxima between the powered electrode and its ground shield, or postpone its formation to higher pressures. Thus smaller gaps result in increased radial uniformity over a wider pressure range. Decreasing the gap also extends the pressure range over which the CF<sub>2</sub> density remains relatively constant with pressure.

The pressure dependence of the optical data are correlated with rf current measurements. At pressures where radially uniform CF<sub>2</sub> distributions and high values of CF<sub>2</sub> at the radial center are observed, the rf current at the grounded electrode is a large fraction of the rf current at the powered electrode. Such conditions, where a large fraction of the rf current flows directly across the electrode gap, result in more radially uniform heating of electrons and more radially uniform production of CF<sub>2</sub>. On the other hand, at fixed pressure, the change in CF<sub>2</sub> density for different electrode gaps is not well correlated to rf current measurements. When the electrode gap is decreased and the pressure held constant, CF<sub>2</sub> density at the radial center generally decreases, whereas the current at the grounded electrode increases. This decline in CF<sub>2</sub> density with gap is probably due to increased surface losses of CF<sub>2</sub>, which should increase with increasing surface-to-volume ratio.

Simple analytic models for the plasma resistance and the sheath impedance are able to provide qualitative explanations of and predictions for the behavior observed in mea-

sured optical and electrical data. The bulk plasma resistance, in particular its dependence on pressure and electrode gap, plays an important role in determining the path that rf current takes through the discharge and the resulting plasma spatial properties. Accurate quantitative predictions of plasma spatial and electrical properties, however, would require more modeling work, perhaps including complete 2D plasma simulations. The results presented here provide necessary data for input and validation of such simulations.

- <sup>1</sup>K. L. Steffens and M. A. Sobolewski, *J. Vac. Sci. Technol. A* **17**, 517 (1999).
- <sup>2</sup>M. A. Sobolewski and K. L. Steffens, *J. Vac. Sci. Technol. A* **17**, 3281 (1999).
- <sup>3</sup>J. P. Booth, G. Cunge, P. Chabert, and N. Sadeghi, *J. Appl. Phys.* **85**, 3097 (1999).
- <sup>4</sup>G. Cunge and J. P. Booth, *J. Appl. Phys.* **85**, 3952 (1999).
- <sup>5</sup>G. A. Hebner, *J. Appl. Phys.* **89**, 900 (2001).
- <sup>6</sup>M. Nakamura, M. Hori, T. Goto, M. Ito, and N. Ishii, *J. Vac. Sci. Technol. A* **19**, 2134 (2001).
- <sup>7</sup>M. Haverlag, W. W. Stoffels, E. Stoffels, G. M. W. Kroesen, and F. J. de Hoog, *J. Vac. Sci. Technol. A* **14**, 384 (1996).
- <sup>8</sup>K. H. R. Kirmse, A. E. Wendt, S. B. Disch, J. Z. Wu, I. C. Abraham, J. A. Meyer, R. A. Breun, and R. C. Woods, *J. Vac. Sci. Technol. B* **14**, 710 (1996).
- <sup>9</sup>Y. Matsumi, S. Toyoda, T. Hayashi, M. Miyamura, H. Yoshikawa, and S. Komiya, *J. Appl. Phys.* **60**, 4102 (1986).
- <sup>10</sup>N. E. Capps, N. M. Mackie, and E. R. Fisher, *J. Appl. Phys.* **84**, 4736 (1998).
- <sup>11</sup>D. S. King, P. K. Schenck, and J. C. Stephenson, *J. Mol. Spectrosc.* **78**, 1 (1979).
- <sup>12</sup>J. P. Booth and G. Hancock, *Chem. Phys. Lett.* **150**, 457 (1988).
- <sup>13</sup>M. A. Lieberman and A. J. Lichtenberg, *Principles of Plasma Discharges and Materials Processing* (Wiley, New York, 1994).
- <sup>14</sup>P. J. Hargis, Jr., K. E. Greenberg, P. A. Miller, J. B. Gerardo, J. R. Torczynski, M. E. Riley, G. A. Hebner, J. R. Roberts, J. K. Olthoff, J. R. Whetstone, R. J. Van Brunt, M. A. Sobolewski, H. M. Anderson, M. P. Splichal, J. L. Mock, P. Bletzinger, A. Garscadden, R. A. Gottscho, G. Selwyn, M. Dalvie, J. E. Heidenreich, J. W. Betterbaugh, M. L. Brake, M. L. Passow, J. Pender, A. Lujan, M. E. Elta, D. B. Graves, H. H. Sawin, M. J. Kushner, J. T. Verdeyen, R. Horwath, and T. R. Turner, *Rev. Sci. Instrum.* **65**, 140 (1994).
- <sup>15</sup>M. A. Sobolewski, *IEEE Trans. Plasma Sci.* **23**, 1006 (1995).
- <sup>16</sup>B. K. McMillin and M. R. Zachariah, *J. Vac. Sci. Technol. A* **15**, 230 (1997).
- <sup>17</sup>M. Haverlag, E. Stoffels, W. W. Stoffels, G. M. W. Kroesen, and F. J. de Hoog, **14**, 380 (1996).
- <sup>18</sup>B. Yip, M. F. Miller, A. Lozano, and R. K. Hanson, *Exp. Fluids* **17**, 330 (1994).
- <sup>19</sup>A. Lozano, B. Yip, and R. K. Hanson, *Exp. Fluids* **13**, 369 (1992).
- <sup>20</sup>K. L. Steffens and M. A. Sobolewski, *IEEE Trans. Plasma Sci.* **27**, 74 (1999).
- <sup>21</sup>M. A. Sobolewski, J. G. Langan, and B. S. Felker, *J. Vac. Sci. Technol. B* **16**, 173 (1998).
- <sup>22</sup>V. A. Godyak, R. B. Piejak, and B. M. Alexandrovich, *IEEE Trans. Plasma Sci.* **19**, 660 (1991).
- <sup>23</sup>M. A. Sobolewski, *Phys. Rev. E* **59**, 1059 (1999).
- <sup>24</sup>L. J. Overzet and F. Y. Leong-Rousey, *Plasma Sources Sci. Technol.* **4**, 432 (1995).
- <sup>25</sup>M. A. Lieberman, *IEEE Trans. Plasma Sci.* **16**, 638 (1988).
- <sup>26</sup>J. G. Langan, S. E. Beck, B. S. Felker, and S. W. Rynders, *J. Appl. Phys.* **79**, 3886 (1996).
- <sup>27</sup>W. R. Entley, J. G. Langan, B. S. Felker, and M. A. Sobolewski, *J. Appl. Phys.* **86**, 4825 (1999).